

Orbital Fingerprint of Topological Fermi Arcs in a Weyl Semimetal

Chul-Hee Min,¹ Hendrik Bentmann,^{1,*} Jennifer N. Neu,² Philipp Eck,³ Simon K. Moser,⁴ Tim Figgemeier,¹ Maximilian Ünzelmann,¹ Katharina Treiber,¹ Peter Lutz,¹ Roland Koch,⁴ Chris Jozwiak,⁴ Aaron Bostwick,⁴ Eli Rotenberg,⁴ Ronny Thomale,³ Giorgio Sangiovanni,³ Theo Siegrist,^{5,2} Domenico Di Sante,³ and Friedrich Reinert¹

¹*Experimentelle Physik VII, Universität Würzburg, Am Hubland, D-97074 Würzburg, Germany*

²*National High Magnetic Field Laboratory, Tallahassee, FL 32310, USA*

³*Theoretische Physik I, Universität Würzburg, Am Hubland, D-97074 Würzburg, Germany*

⁴*Advanced Light Source, Lawrence Berkeley National Laboratory, Berkeley, CA 94720, USA*

⁵*Department of Chemical and Biomedical Engineering,
FAMU-FSU College of Engineering Tallahassee, FL 32310, USA*

(Dated: May 10, 2022)

Weyl semimetals are characterized by Fermi arc surface states. As a function of surface momentum, such arcs constitute energy-degenerate line trajectories terminating at the surface projection of two bulk Weyl nodes with opposite chirality¹⁻⁶. At these projection points, the Fermi arc transcends into a bulk state, and as such yields an intricate connectivity of surface-localized and bulk-delocalized states⁷⁻⁹. Spectroscopic approaches face the challenge to efficiently image this surface-bulk transition of the Fermi arcs for topological semimetals in general. Here, employing a joint analysis from orbital-selective angle-resolved photoemission and first-principles calculations, we unveil the orbital texture on the full Fermi surface of TaP. We put forward a diagnosis scheme to formulate and measure the orbital fingerprint of topological Fermi arcs and their surface-bulk transition in a Weyl semimetal.

The discovery of topological insulators gave birth to the present field of topological quantum states in crystalline solids¹⁰. In a recent breakthrough, the notion of topological phases of matter was extended from insulators to gapless semimetals^{1,2,9,11}. A paradigmatic example is the Weyl semimetal^{5,6}, whose band structure features topologically protected band touching points near the Fermi level, called Weyl nodes.

Probably the most striking manifestation of the topological properties in a Weyl semimetal is the existence of unconventional Fermi-arc surface states. As a function of surface momentum, these states form non-closed Fermi-surface segments that connect to the surface projections of two bulk Weyl nodes of opposite chirality^{1,2}. Near such projected Weyl nodes, the Fermi arc transcends into a bulk state and its wave function delocalizes into the bulk of the crystal. This transcendence regime is fundamental to the topological physics of Weyl semimetals, and it underlies unique electronic¹² and spectroscopic¹³ phenomena in topological semimetals in general, such as non-local Weyl orbits¹⁴.

In this work we reveal the critical role of the orbital degree of freedom in mediating the topological surface-bulk connectivity in Weyl semimetals. Employing angle-resolved photoemission experiments and first-principles calculations, we unveil a complex orbital texture of the Fermi surface in the

Weyl semimetal TaP. Our measurements evidence rapid rearrangements in orbital composition of the surface states near projected Weyl nodes, and show that arcs connecting different pairs of Weyl points feature distinct orbital symmetries.

Previous works on topological insulators and topological crystalline insulators uncovered the importance of orbital textures for a realistic description of the topological surface states and a variety of their properties^{10,15-18}. In Weyl semimetals, pronounced modulations of the Fermi-arc spin texture near projected Weyl points⁸ as well as a highly momentum-dependent orbital texture¹⁹ have been predicted by first-principles calculations. Yet, experimentally such orbital dependences in the surface electronic structure of Weyl semimetals have remained elusive.

TaP crystallizes in the non-centrosymmetric space group $I4_1md$, as shown in Fig. 1a. Its bulk band structure features 24 Weyl points in the Brillouin zone^{3-6,8,20-22}. A projection on the (001) plane gives rise to two inequivalent sets of projected Weyl points, W_1 and W_2 . The calculated band structure of the P-terminated TaP(001) surface in Fig. 1d highly accurately matches with our ARPES measurements in Fig. 1e-f, in particular regarding the bands close to the Fermi level which are relevant for the topological properties. In turn, by comparing theory and experiment, we identify all main spectral features in the experimental data as surface states. The calculated Fermi surface of TaP(001) in Fig. 1b is composed of the spoon-shaped feature α , the neck feature β , as well as the outer bowtie-shaped feature γ around the \bar{X} - and \bar{Y} -points. As seen in Fig. 1b, the projected Weyl nodes W_2 and W_1 are located approximately at the connection points of the features α and β as well as γ and β , respectively.

Based on the precise consistency of the experimental and theoretical band structures, we shall now address the orbital composition of the Fermi-arc surface states. To this end we make use of parity selection rules within the dipole approximation for photoexcitation with linearly polarized light^{16,18}. The experimental geometry is shown in Fig. 1c, in which the light electric field vector is given by $(0, \mathcal{E}_y, 0)$ for s -polarization and by $(\mathcal{E}_x, 0, \mathcal{E}_z)$ for p -polarization. We acquired ARPES data as a function of both in-plane momentum components without changing the experimental geometry by employing

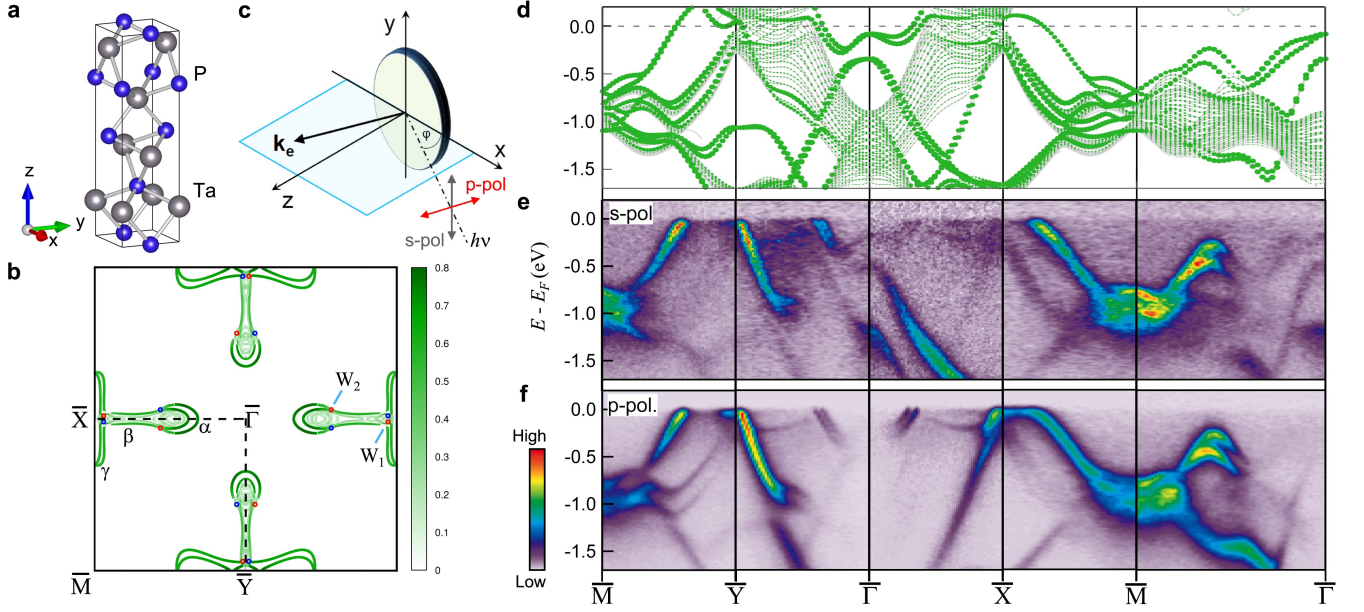


Figure 1: **Surface electronic structure of the Weyl semimetal TaP(001).** **a**, Bulk crystal structure of TaP with space group $I4_1md$. **b**, Calculated Fermi surface of the P-terminated TaP(001) surface with C_{2v} symmetry. The features α , β and γ as well as the positions of the projected Weyl points W_1 and W_2 are indicated. **c**, Experimental geometry of the angle-resolved photoemission (ARPES) experiment with linearly polarized light. **d-f**, Band structure of P-terminated TaP(001) along high-symmetry directions, as determined by a first-principles calculation and by ARPES using s - and p -polarized light at $h\nu = 105$ eV. In **d** the size of the green dots highlights the orbital contribution from the atoms in the surface unit-cell.

custom-made deflectors. Using p -polarized light, incident along the emission plane, only even orbital components of the initial state contribute to the photoemission intensity, while for s -polarized light only odd components contribute. As indicated by arrows in Fig. 2a-d, for different light polarizations we observe pronounced intensity variations in the measured Fermi-surface contours close to the projected bulk Weyl points W_1 and W_2 [cf. Fig. 1b]. We will show in the following how these variations reflect characteristic orbital-texture modulations of the topological Fermi arcs.

For s -polarized light the intensity of the states α and γ is almost entirely suppressed along k_x , i.e. within the plane of light incidence (Fig 2c-d). This suppression persists over a wide range of excitation energies (see supplementary note I), demonstrating that it is independent of the photoelectron final state and related to the symmetry of the initial state. From the experimental data, we therefore infer an almost purely even orbital symmetry for the states α and γ relative to the xz mirror plane. This pure orbital symmetry of the Fermi-arc states is in striking contrast to the orbital wave-function of the surface states in topological insulators that show a strong mixing of even and odd orbital components^{16,18}.

Our first-principles calculations in Fig. 2 confirm the experimentally determined orbital symmetry. Along k_x the state α is composed predominantly of Ta $d_{x^2-y^2}$ and P p_x orbitals, and the state γ consists mainly of P p_z and Ta d_{z^2} out-of-plane orbitals.¹⁹ Hence, while both features derive from even orbitals, the overall orbital texture on the Fermi sur-

face varies from out-of-plane near the Brillouin zone boundary towards in-plane near the center. This is corroborated by the photon-energy-dependent ARPES data in Fig. 2e obtained with p -polarized light. Along either $+k_x$ or $-k_x$, the state α shows complete intensity suppressions over several intervals of photon energy. Such a pronounced linear dichroism can be attributed to the sizable in-plane p_x orbital component of α ,^{23,24} mainly coupling to the in-plane component \mathcal{E}_x of the light electric field. By contrast, \mathcal{E}_x is expected to couple less strongly to out-of-plane d_{z^2} and p_z orbitals, as reflected by the weaker dichroism for γ .

Considering next the full momentum dependence of the ARPES data sets, we find that the intensity distributions obtained with s -polarized light in Fig. 2c-d show sharp changes near the W_2 Weyl points, where the spoon feature α evolves into the neck feature β . In particular, along k_x the intensity of α is suppressed while β shows appreciable intensity. Our calculations in Fig. 2f demonstrate how this is related to rapid changes of the Fermi-arc orbital texture near W_2 . Specifically, we find a dominating odd d_{yz} orbital component for β as opposed to the predominantly even orbitals contributing to α . By contrast, along k_y the intensity quickly increases when passing through W_2 from β to α . This is in line with the large p_y orbital contribution for α that couples to the \mathcal{E}_y component of the s -polarized light.

In the Fermi surfaces measured with p -polarized light in Fig. 2a-b we also observe pronounced intensity variations near the W_2 points, as indicated by arrows, further substantiating

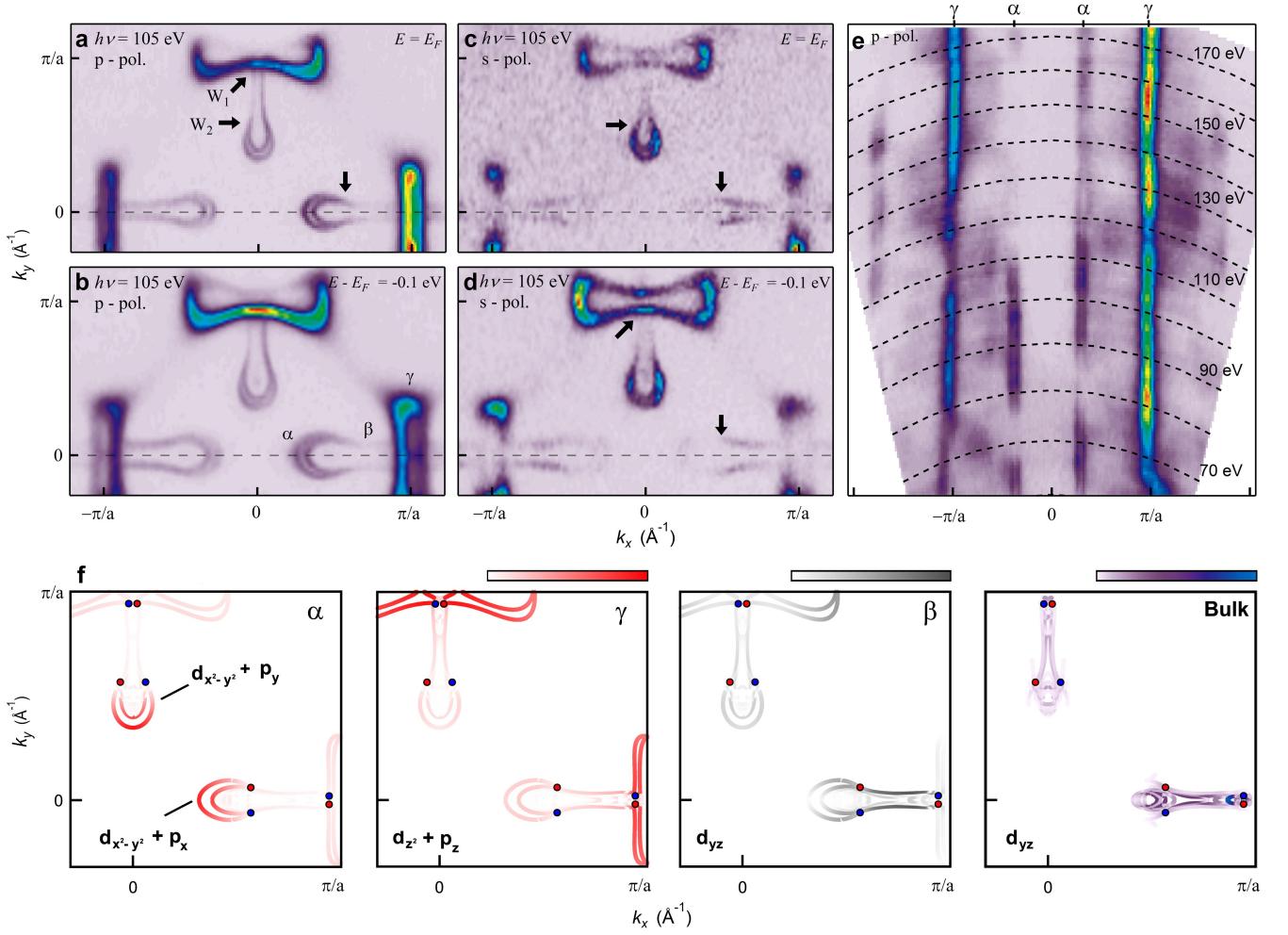


Figure 2: Orbital texture of the Fermi arcs in TaP(001). **a-d**, ARPES constant-energy-contours of the surface band structure at the Fermi level E_F and at $E - E_F = -0.1$ eV obtained with s - and p -polarized light. In the vicinity of the projected Weyl points W_1 and W_2 [cf. Fig. 1b] pronounced changes in the ARPES intensity are observed (indicated by arrows), evidencing pronounced rearrangements in the orbital composition. **e**, Photon-energy-dependence of the ARPES intensity at E_F and $k_y = 0$ for p -polarized light. **f**, Calculated Fermi surface projected on different Ta 5d and P 3p orbitals in the surface unit cell. A projection on the d_{yz} orbital is shown for a unit cell in the bulk.

the change in orbital nature of the Fermi arcs. Moreover, close to the projected W_1 Weyl points, where γ evolves into β , the ARPES data show similarly pronounced intensity changes as near W_2 . This observation is in line with our first-principles calculations revealing an abrupt change in orbital character near W_1 from d_{z^2} and p_z for γ to mainly d_{yz}/d_{xz} for β . A full set of the calculated orbital-projected Fermi surfaces in the bulk and at the surface is given in supplementary note II.

The fact that the observed orbital-texture changes occur in close proximity to the projected Weyl points indicates that these changes arise from the topological connectivity of the Fermi arcs and the bulk band structure^{7,9}. Our calculations in Fig. 3 indeed show how the reorganization of the orbital wave function is directly linked to the momentum-dependent bulk propagation of the Fermi arcs. The states α and γ are well-separated in momentum space from the projected bulk Fermi surface, protecting them from delocalization into the crystal volume¹³. Their wave functions are, accordingly, highly

surface-localized and have a large contribution of dangling p orbitals of the surface P atoms¹³. Near the projected Weyl points, the wave functions propagate deep into the bulk, as directly seen in Fig. 3b.

By comparing the orbital character on the bulk and the surface Fermi surface, we find that, in the course of approaching the projected bulk continuum, the surface states adjust their orbital symmetry to the one of nearby bulk states, as shown explicitly for the d_{yz} orbital component in Fig. 2f. Note that, in general, a surface state may retain its surface localization even when dispersing through a projected bulk continuum, as long as the surface and bulk states feature distinct symmetries²⁵. In this regard, it is the adjustment in orbital symmetry to the continuum states that allows the Fermi-arc surface states to delocalize into the bulk and to merge with the Fermi-arcs of the opposite surface.

While orbital-related phenomena in the electronic structure of

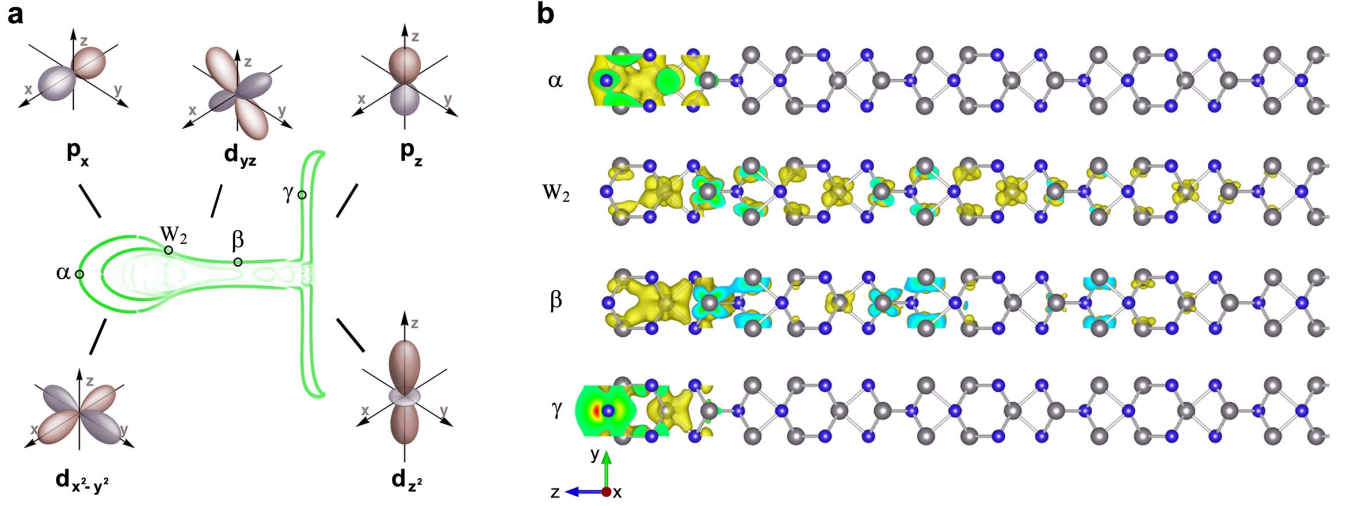


Figure 3: Orbital fingerprint and bulk propagation of the Fermi arcs in TaP(001). **a**, Calculated Fermi surface with schematic indications of the varying orbital character deduced from the orbital-selective ARPES experiments and first-principles calculations in Fig. 2. The spoon-shaped feature α arises mainly from in-plane $d_{x^2-y^2}$ and p_x orbitals, and the bowtie feature γ is derived from out-of-plane p_z and d_{z^2} orbitals. The neck feature β shows mixed Ta d orbital character with a dominating d_{yz} component. **b**, Partial charge densities of the Fermi arcs calculated at four selected positions on the Fermi surface indicated in **a**. The states α and γ are highly localized in the first few atomic layers of the surface, while near the W_2 Weyl point and for the state β the surface-state wave function propagates deep into the bulk.

topological and strongly correlated materials have been extensively discussed recently^{15–18,26–28}, the orbital-texture characteristics of topological Fermi arcs, reported here, are distinct in that they arise from the non-trivial connectivity of surface and bulk band structure. The latter is a hallmark feature of topological semimetals and underlies unusual electron transport phenomena in these materials^{12,14}. The present results establish the analysis of orbital textures as a way to distinguish the surface and bulk character of electronic states in topological semimetals.

Our experiments and calculations reveal pronounced variations of the Fermi-arc orbital character arising from the topological connectivity to the bulk band structure. Given the inherently strong spin-orbit coupling in TaP and related Weyl semimetals, these variations in orbital composition will also affect the spin polarization of the Fermi arcs. Modulations of the Fermi-arc spin texture near projected Weyl nodes, similar to the ones observed here for the orbital texture, have indeed been predicted theoretically⁸. Pioneering works demonstrated a spin polarization of the Fermi arcs^{19,29}, and novel spin-imaging ARPES experiments^{30,31} might be able to reveal such spin-texture modulations across momentum space, when combined with the orbital-selective excitation of the Fermi arcs demonstrated here. In view of previous findings of orbital-dependent Dirac states in topological insulators¹⁶ and topological crystalline insulators¹⁷, we expect that the orbital nature of the Fermi arcs will also manifest itself in their scattering properties. Orbital-dependent coherent scattering has been observed in quasi-particle interference imaging of topological crystalline insulators and other spin-orbit compounds^{17,32}. For the presently studied Fermi arcs, such orbital-dependences might complement or even enhance pre-

viously reported effects related to the momentum-dependent bulk delocalization of the wave function¹³.

I. METHODS

TaP single crystals were prepared via chemical vapour transport in sealed silica ampoules. The ampoules were loaded with a stoichiometric ratio of tantalum (foil) to red phosphorus (chunks), such that the total reaction mass was 1 g. Elemental iodine ($\sim 2.5 \text{ mg/cm}^3$) was added, and the ampoules were sealed under vacuum ($\sim 70 \text{ mTorr}$). The ampoules were then tilted $\sim 20^\circ$ from the horizontal as indicated by Li *et al.*³³ and placed in a single zone tube furnace with a defined temperature gradient. The ampoules were heated at 5°C/hr to 500°C , held at 500°C for 24 hours, and then heated to 1000°C at 5°C/hr . They were placed in a temperature gradient ($T_H:T_C = 1000^\circ\text{C}:940^\circ\text{C}$) for approximately 3 weeks and then cooled to room temperature by switching off the furnace. Tetragonal crystals of TaP as large as 1 mm^3 were obtained by this method. Single crystal x-ray diffraction³⁴ confirmed the phase and the stoichiometry was verified by EDS (Zeiss 1540 XB Crossbeam Scanning Electron Microscope).

We performed ARPES experiments on the TaP single crystals at the Microscopic And Electronic STRucture Observatory (MAESTRO) at beamline 7 of the Advanced Light Source (ALS) in the photon energy range of $60 \text{ eV} - 180 \text{ eV}$. The slit of a Scienta R4000 electron analyzer was aligned in the plane of light incidence, namely the xz -plane as shown in Fig. 1(c). The ARPES data were collected using custom-made deflectors which enable collecting ARPES spectra over a full Brillouin zone without moving the sample and thus al-

low to retain the X-ray focus on small sample domains. The total energy and momentum resolutions were ≤ 30 meV and 0.01 \AA^{-1} . Measurements were performed in ultra-high vacuum of lower than 1×10^{-10} mbar for the samples cooled down below 20 K.

For the theoretical study of TaP we considered a supercell made of 7 repetitions of the unit cell along the (001) direction and applied first-principles calculations based on density functional theory (DFT) as implemented in the Vienna ab initio simulation package (VASP)³⁵. The projector-augmented-plane-wave (PAW) method was used by expanding the Kohn-Sham wavefunctions into plane waves to an energy cut-off of 300 eV³⁶. Spin-orbit coupling was included self-consistently and the exchange-correlation was computed within the generalized gradient approximation as parameterized in the PBE-GGA functional³⁷. For the self-consistent computation we sampled the Brillouin zone on a $14 \times 14 \times 1$ k-point mesh, while we used a finer grid of at least 256×256 points for the Fermi surfaces. The unit-cell parameters used in the calculation were $a = 3.32 \text{ \AA}$ and $c = 11.34 \text{ \AA}$. The vacuum layer had a thickness of 11.90 Å. The surface and bulk character were obtained by projecting on the atomic Ta- and P-orbitals in the topmost and in the fourth unit cell, respectively. In order to match the experimental chemical potential the calculated band structure was shifted rigidly by 50 meV to higher energy. The surface bands of the Ta-terminated slab side were removed in the figures of the main text, see supplementary note III.

II. ACKNOWLEDGMENTS

H.B. would like to thank Jan Minar for helpful discussions. This work was supported by the DFG through SFB1170 'Tocotronics', RE 1469/13-1, and through SPP-1666, and by ERC-StG-336012-Thomale-TOPOLECTRICS. We gratefully acknowledge the Gauss Centre for Supercomputing e.V. (www.gauss-centre.eu) for funding this project by providing

computing time on the GCS Supercomputer SuperMUC at Leibniz Supercomputing Centre (www.lrz.de). J.N and T.S. acknowledge support from the National Research Foundation, under grant NSF DMR-1606952. The crystal synthesis and characterization was carried out at the National High Magnetic Field Laboratory, which is supported by the National Science Foundation, Division of Materials Research under grants DMR-1157490 and DMR-1644779, the state of Florida and Florida State University. S.M. acknowledges support by the Swiss National Science Foundation (grant no. P300P2-171221). This research used resources of the Advanced Light Source, which is a US Department of Energy Office of Science User Facility under contract no. DE-AC02-05CH11231.

III. AUTHOR CONTRIBUTIONS

ARPES measurements: C.-H.M., S.M., P.L., K.T.; Sample growth and characterization: J.N, T.S.; Data analyses and Interpretation: C.-H.M., H.B., P.E., D.D.S, G.S., R.T. ; DFT calculations: P.E., D.D.S. with input from G. S., R.T.; Writing of the manuscript and project conception: H.B. with input from C.-H.M., F.R., S.M., D.D.S, G.S, R.T.; The microARPES set-up was developed and maintained by R.K, C.J., A.B. and E.R. All authors discussed extensively the results and the manuscript.

IV. ADDITIONAL INFORMATION

The authors declare no competing financial interests. Correspondence and requests for materials should be addressed to Hendrik Bentmann (e-mail: hendrik.bentmann@physik.uni-wuerzburg.de).

* Electronic address: Hendrik.Bentmann@physik.uni-wuerzburg.de

- ¹ Wan, X., Turner, A. M., Vishwanath, A. & Savrasov, S. Y. Topological semimetal and Fermi-arc surface states in the electronic structure of pyrochlore iridates. *Phys. Rev. B* **83**, 205101 (2011).
- ² Burkov, A. A. & Balents, L. Weyl Semimetal in a Topological Insulator Multilayer. *Phys. Rev. Lett.* **107**, 127205 (2011).
- ³ Huang, S.-M. *et al.* A Weyl Fermion semimetal with surface Fermi arcs in the transition metal monophenide TaAs class. *Nature Communications* **6** (2015).
- ⁴ Weng, H., Fang, C., Fang, Z., Bernevig, B. A. & Dai, X. Weyl Semimetal Phase in Noncentrosymmetric Transition-Metal Monophosphides. *Phys. Rev. X* **5**, 011029 (2015).
- ⁵ Xu, S.-Y. *et al.* Discovery of a Weyl fermion semimetal and topological Fermi arcs. *Science* **349**, 613–617 (2015).
- ⁶ Lv, B. Q. *et al.* Experimental Discovery of Weyl Semimetal TaAs. *Phys. Rev. X* **5**, 031013 (2015).
- ⁷ Turner, A. M. & Vishwanath, A. Beyond Band Insulators: Topol-

ogy of Semimetals and Interacting Phases. *Contemporary Concepts of Condensed Matter Science* **6**, 293–324 (2013).

- ⁸ Sun, Y., Wu, S.-C. & Yan, B. Topological surface states and Fermi arcs of the noncentrosymmetric Weyl semimetals TaAs, TaP, NbAs, and NbP. *Phys. Rev. B* **92**, 115428 (2015).
- ⁹ Armitage, N. P., Mele, E. J. & Vishwanath, A. Weyl and Dirac semimetals in three-dimensional solids. *Rev. Mod. Phys.* **90**, 015001 (2018).
- ¹⁰ Hasan, M. Z. & Kane, C. L. *Colloquium*: Topological insulators. *Rev. Mod. Phys.* **82**, 3045–3067 (2010).
- ¹¹ Bradlyn, B. *et al.* Beyond Dirac and Weyl fermions: Unconventional quasiparticles in conventional crystals. *Science* **353** (2016).
- ¹² Potter, A. C., Kimchi, I. & Vishwanath, A. Topological semimetal and Fermi-arc surface states in the electronic structure of pyrochlore iridates. *Nat. Commun.* **5**, 5161 (2014).
- ¹³ Inoue, H. *et al.* Quasiparticle interference of the Fermi arcs and surface-bulk connectivity of a Weyl semimetal. *Science* **351**, 1184–1187 (2016).

- ¹⁴ Moll, P. J. W. *et al.* Transport evidence for Fermi-arc-mediated chirality transfer in the Dirac semimetal Cd_3As_2 . *Nature* **535**, 266 (2016).
- ¹⁵ Park, S. R. *et al.* Chiral Orbital-Angular Momentum in the Surface States of Bi_2Se_3 . *Phys. Rev. Lett.* **108**, 046805 (2012).
- ¹⁶ Cao, Y. *et al.* Mapping the orbital wavefunction of the surface states in three-dimensional topological insulators. *Nature Physics* **9**, 499–504 (2013).
- ¹⁷ Zeljkovic, I. *et al.* Mapping the unconventional orbital texture in topological crystalline insulators. *Nature Physics* **10**, 572–577 (2014).
- ¹⁸ Xie, Z. *et al.* Orbital-selective spin texture and its manipulation in a topological insulator. *Nature Communications* **5**, 4382 (2014).
- ¹⁹ Xu, S.-Y. *et al.* Spin Polarization and Texture of the Fermi Arcs in the Weyl Fermion Semimetal TaAs. *Phys. Rev. Lett.* **116**, 096801 (2016).
- ²⁰ Xu, N. *et al.* Observation of Weyl nodes and Fermi arcs in tantalum phosphide. *Nature Communications* **7**, 11006 (2016).
- ²¹ Xu, S.-Y. *et al.* Experimental discovery of a topological Weyl semimetal state in TaP. *Science Advances* **1** (2015).
- ²² Liu, Z. K. *et al.* Evolution of the Fermi surface of Weyl semimetals in the transition metal pnictide family. *Nature Materials* **15**, 4457 (2015).
- ²³ Henk, J., Hoesch, M., Osterwalder, J., Ernst, A. & Bruno, P. Spin-orbit coupling in the L-gap surface states of Au(111): spin-resolved photoemission experiments and first-principles calculations. *Journal of Physics: Condensed Matter* **16**, 7581 (2004).
- ²⁴ Bentmann, H. *et al.* Strong Linear Dichroism in Spin-Polarized Photoemission from Spin-Orbit-Coupled Surface States. *Phys. Rev. Lett.* **119**, 106401 (2017).
- ²⁵ Kerker, G. P., Ho, K. M. & Cohen, M. L. Mo(001) Surface: A Self-Consistent Calculation of the Electronic Structure. *Phys. Rev. Lett.* **40**, 1593–1596 (1978).
- ²⁶ Wiessner, M. *et al.* Complete determination of molecular orbitals by measurement of phase symmetry and electron density. *Nature Communications* **5**, 4156 (2014).
- ²⁷ Ritschel, T. *et al.* Orbital textures and charge density waves in transition metal dichalcogenides. *Nature Physics* **11**, 328–331 (2015).
- ²⁸ Borisenko, S. V. *et al.* Direct observation of spinorbit coupling in iron-based superconductors. *Nature Physics* **12**, 311–317 (2016).
- ²⁹ Lv, B. Q. *et al.* Observation of Fermi-Arc Spin Texture in TaAs. *Phys. Rev. Lett.* **115**, 217601 (2015).
- ³⁰ Tusche, C., Krasnyuk, A. & Kirschner, J. Spin resolved bandstructure imaging with a high resolution momentum microscope. *Ultramicroscopy* **159**, 520–529 (2015).
- ³¹ Maaß, H. *et al.* Spin-texture inversion in the giant Rashba semiconductor BiTeI. *Nature Communications* **7**, 11621 (2016).
- ³² El-Kareh, L. *et al.* A combined experimental and theoretical study of Rashba-split surface states on the $(\sqrt{3} \times \sqrt{3}) \text{Pb/Ag}(111)R30^\circ$ surface. *New Journal of Physics* **16**, 045017 (2014).
- ³³ Li, Z. *et al.* Weyl Semimetal TaAs: Crystal Growth, Morphology, and Thermodynamics. *Crystal Growth & Design* **26**, 1172–1175 (2016).
- ³⁴ Rigaku Oxford Diffraction, CrysAlisPro Software system (version 1.171.38.43), Rigaku Corporation, Oxford, UK (2016).
- ³⁵ Kresse, G. & Furthmüller, J. Efficient iterative schemes for ab initio total-energy calculations using a plane-wave basis set. *Phys. Rev. B* **54**, 11169–11186 (1996).
- ³⁶ Kresse, G. & Joubert, D. From ultrasoft pseudopotentials to the projector augmented-wave method. *Phys. Rev. B* **59**, 1758–1775 (1999).
- ³⁷ Perdew, J. P., Burke, K. & Ernzerhof, M. Generalized Gradient Approximation Made Simple. *Phys. Rev. Lett.* **77**, 3865–3868 (1996).